Materiales de Construcción
Vol. 73, Issue 349, January-March 2023, e309
ISSN-L: 0465-2746
https://doi.org/10.3989/mc.2023.296622

Demanda Gold sandstone (Burgos): effect of consolidation and ageing tests on its petrographic and petrophysical properties

A. Gómez-Marfil[a,b]✉, M.J. Varas-Muriel[a,b]

a. Facultad de Ciencias Geológicas, Universidad Complutense de Madrid, (Madrid, Spain)
b. Instituto de Geociencias (CSIC-UCM), (Madrid, Spain)
✉: amagom01@ucm.es

Received 16 June 2022
Accepted 04 October 2022
Available on line 06 March 2023

ABSTRACT: Sandstones have been widely used in construction for their abundance, aesthetics, and ease of extraction. To determine sandstones' quality, it is essential to analyse their petrographic and petrophysical properties and sensitivity (durability and conservation) to environmental agents. This paper evaluates the physical-mechanical changes undergone by Sierra de la Demanda (Burgos, Spain) sandstone under combined and induced water and salt aggression and assesses ESTEL 1100's effectiveness and suitability as a treatment. This sandstone is porous, permeable, dense and quartz-rich with high hardness and strength. The treatment improved its petrophysical properties by modifying its pore geometry and connectivity, reducing absorbency, permeability and anisotropy, and further increasing its hardness and resistance. Salts did not substantially modify its properties as its porosity type absorbed the crystallisation pressure. Ultimately, its pore system and predominantly quartz composition make it a high-quality, weather-resistant material compatible with the treatment applied.

KEY WORDS: Sandstone; Quality; Durability; Porosity; Petrographic and petrophysical characterisation.

Citation/Citar como: Gómez-Marfil, A.; Varas-Muriel, M.J. (2023) Demanda Gold sandstone (Burgos): effect of consolidation and ageing tests on its petrographic and petrophysical properties. Mater. Construcc. 73 [349], e309. https://doi.org/10.3989/mc.2023.296622.

RESUMEN: *Arenisca Dorada de la Demanda (Burgos): efecto de ensayos de consolidación y envejecimiento en sus propiedades petrográficas y petrofísicas.* Las areniscas han sido uno de los materiales de construcción más utilizados por su abundancia, estética y fácil extracción. Para determinar su calidad es esencial analizar sus propiedades petrográficas y petrofísicas, así como su sensibilidad (durabilidad y conservación) a los agentes medioambientales. Este trabajo evalúa tanto los cambios físico-mecánicos sufridos por una arenisca de la Sierra de la Demanda (Burgos, España), ante la agresión combinada e inducida de agua y sales, como la eficacia e idoneidad del tratamiento ESTEL 1100. Esta arenisca es porosa, permeable, densa, rica en cuarzo, y con alta dureza y resistencia. El tratamiento mejoró sus propiedades petrofísicas, modificando la geometría y conectividad de sus poros, y reduciendo su absorción, permeabilidad y anisotropía. Las sales no modificaron sustancialmente sus propiedades, ya que su porosidad absorbió su presión de cristalización. El sistema poroso y el abundante cuarzo hacen de esta arenisca un material de alta calidad, resistente a la intemperie y compatible con el tratamiento aplicado.

PALABRAS CLAVE: Arenisca; Calidad; Durabilidad; Porosidad; Caracterización petrográfica y petrofísica.

Copyright: ©2023 CSIC. This is an open-access article distributed under the terms of the Creative Commons Attribution 4.0 International (CC BY 4.0) License.

1. INTRODUCTION

Sandstones are sedimentary, granular, porous rocks widely used in construction worldwide because of their great abundance on the planet's surface, ease of extraction and processing and high aesthetic value. However, sandstones are soft materials likely to suffer severe weathering when exposed to environmental agents (1-7). Sandstones' great compositional and textural variety means their physical and mechanical behaviour differs widely. It is therefore necessary to characterise their petrographic and petrophysical parameters in order to assess their quality as a building material and predict their medium- and long-term behaviour and durability (2, 3, 7-12).

The presence of specific mineralogy in sandstones' intergranular space (clay matrices and/or crystalline cement), as well as the empty spaces that define their pore system, are the main features that determine these materials' hardness and thus their quality and durability as they constrain sandstones' intergranular cohesion and resistance to aggression from the two most damaging agents of deterioration: water and salts (2, 3, 6, 9, 13-16). The side effects of water circulation and the crystallisation pressure exerted by soluble salts within the pore system of any material will cause significant changes in pore size, geometry, quantity and distribution. These in turn produce measurable changes in the material's petrophysical properties (3-5, 15, 17–20).

Laboratory simulations, such as accelerated ageing tests, are carried out in order to assess the type and extent of damage these stones suffer under real environmental conditions. These tests are usually destructive in the short term, which makes it possible to compare the induced damage with the real damage and thus estimate the degree of durability (1, 7, 9). Although most durability properties can be improved by applying consolidation and/or water-repellent treatments, these products can also be affected by environmental agents (10, 21-23). Treatment use has grown over the last century and the extremely wide variety of products on the market creates uncertainty about their degree of effectiveness and their suitability for the stone to which they are to be applied (24-27).

This paper characterises both the petrographic and petrophysical properties of a porous sandstone marketed as 'Demanda Gold' (Sierra de la Demanda, Burgos, Spain) and the changes in these properties after treating it with ESTEL 1100 and/or subjecting it to accelerated ageing by salt crystallisation in order to establish the aforementioned sandstone's quality and durability as a building material. Likewise, it evaluates the treatment's compatibility with this stone and its effectiveness against the action of water and salts. Analysis will place special emphasis on changes to the pore system.

Demanda Gold sandstone is principally quarried in Palacios de la Sierra, Burgos, Spain (41° 58' 26.37" N, 3° 6' 27.46" W), although it is also extracted in Sala de los Infantes, Vilviestre del Pinar, Canicosa de la Sierra and Quintanar de la Sierra (Burgos). It is known commercially as 'Piedra de la Demanda', 'Dorada Urbión' or 'Piedra de Salas'. This sandstone has historically been used in the towns and villages close to the extraction sites. It is currently marketed nationally and internationally and is found in buildings in Madrid, Burgos, Soria, Salamanca, Cantabria and the Basque Country. It is used in both modern and traditional architecture, mainly as cladding for façades and exterior walls, although it is also used in masonry and ashlars. Geologically, this sedimentary rock is found in the southern domain of the Iberian Mountain Range in the Cameros Basin. It belongs to the Aptian (Lower Cretaceous) Weald facies, which originated during the second rifting phase (28). The sandstones are texturally and compositionally mature and are classified as quartz arenites and subarkoses of a whitish to greyish ochre colour. They are continental-origin detrital facies with lateral facies changes where dry and wet cycles occur, causing the oxidation of ferrous ions and giving rise to red banding (29) typical of the sandstone variety marketed as 'Veteada de la Demanda' (Cream Veined) sandstone (30).

2. METHODOLOGY

2.1 Materials

The Demanda Gold sandstone was supplied by *Areniscas Sierra de la Demanda S.L.*, a company located in Palacios de la Sierra (Burgos). A total of 24 specimens of different dimensions were cut: 12 cubic specimens measuring 5 x 5 x 5 cm and weighing 281.4 ± 10.4 g; 6 prismatic specimens measuring 1 x 1 x 10 cm and weighing 51.5 ± 10.1 g; and 6 flat square plates measuring 5 x 5 x 1 cm and weighing 49.2 ± 5.9 g (Figure 1, Table 1).

The ESTEL 1100 chemical conservation product, provided by *CTS España S.L.*, possesses consolidant and water-repellent properties. It is composed of silicic acid ethyl esters and oligomeric polysiloxanes dissolved in organic solvent. These compounds react with atmospheric moisture to form a silica gel. The reaction takes four weeks to complete according to the manufacturer's specifications. The treatment performs a dual function: 1) it penetrates the material to unite its granular components as a cementitious hardening product and 2) it waterproofs the surface to prevent water ingress. A double coat was applied to half of each type of specimen (cubic, prismatic and plates). No product was applied to the upper and lower faces of the prismatic test specimens in order to facilitate the ascent of water inside them. On the flat specimens, the product was only applied to the outer face exposed to the atmosphere. Product absorption accounted for 1.7–2.5% of the weight of the specimens.

The following abbreviations are used in this paper to refer to each type of sample according to whether they have been treated and/or degraded with salts: Demanda Gold sandstone (ADD), Demanda Gold sandstone with

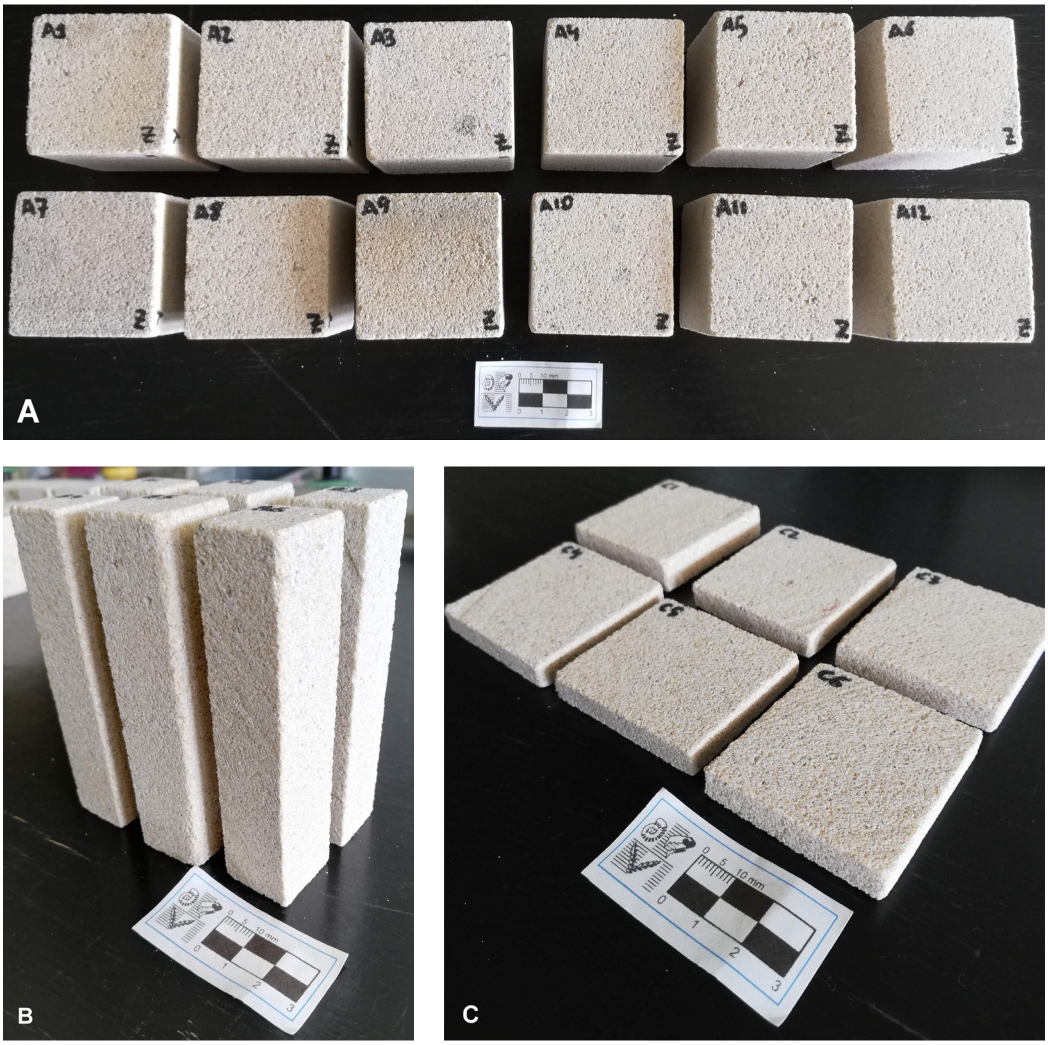

Figure 1. Cut specimens. A: cubic, B: prismatic, C: plates.

Table 1. Summary table of the samples tested. In brackets, the number of specimens of each type according to the process undergone.

		Cubic specimens	Prismatic specimens	Plate specimens
ADD	Original	A7-A12 (6)	B4-B6 (3)	C4-C6 (3)
ADDs	Salts	A7-A9 (3)	B4-B6 (3)	C4-C6 (3)
ADDT	Treatment	A1-A6 (6)	B1-B3 (3)	C1-C3 (3)
ADDTs	Salts + treatment	A1-A3 (3)	B1-B3 (3)	C1-C3 (3)

salts (ADDs), Demanda Gold sandstone with treatment (ADDT) and Demanda Gold sandstone with treatment and salts (ADDTs) (Table 1).

2.2 Techniques and tests

The techniques and tests used in this paper followed the UNE-EN 16515:2016 standard (31) on characterisation of natural stone used in cultural heritage. Both petrographical and petrophysical characterisation were made in two stages, being the first one before the ageing test (ADD, ADDT), and the second one right after it (ADDs, ADDTs).

2.2.1 Petrographical characterisation

Compositional and textural characterisation of the samples were carried out by macroscopic and microscopic description as per the UNE-EN 12407:2020 standard (32). An *Olympus BX51* fluorescence and polarising light microscope (PLM) equipped with an *Olympus U-RFL-T* mercury lamp and *Olympus CellSens Entry v2.3* image acquisition software was used. To facilitate both detection of pores and cracks in thin sections (3 x 2 cm and 30 µm thick), the sandstone samples were impregnated with fluorescent yellow resin (*EpoDye*) (33). The *Oxford Instruments FEI Inspect* scanning electron microscope (SEM) in secondary electron mode (SE) with dispersive energy X-ray detector (EDS) was used to locate the salts and treatment. This equipment was operated under vacuum at a pressure of 0.50 torr and a voltage of 20 kV. Unmetallised fragments < 1 cm^3 were studied. Crystallised mineral phases were detected by X- ray diffraction (XRD) of the fragments' powder fraction (< 53 µm). A *BRUKER D8* diffractometer with CuKα anode and graphite monochromator was used. The measurements were performed on a 2 g powder sample in a range between 2° and 65°, with an interval of 0.02°/min in continuous mode. Fourier transform infrared spectroscopy (FTIR) was used to detect the treatment. The device used was a *Nicolet Nexus 670-870* measuring in the infrared spectrum's 4000–400 cm^{-1} range. *BrK* pellets and a 1.5 mg powder sample were used for this test.

2.2.2 Petrophysical characterisation

Surface properties: The following tests were carried out on the cubic specimens: 1) colour measurement of surfaces (UNE-EN 15886:2011 (34); ASTM E313:2020 (35)) using CIELAB system parameters (1976) and a *Minolta CM-700d* spectrophotometer with D65° illuminant and the *SpectraMagic NX Color Data Software (CM-100SW)*; 2) gloss (ASTM D523-14:2018 (36)) using a *BYK Gardner Multigloss 268* glossmeter; 3) infrared thermography (UNE-EN 16714:2017 (37)) using a *Termacam B4 FLIR* infrared camera; and 4) static contact angle (UNE- EN 15802:2010 (38)) using a *Dino-Lite Edge* digital microscope (AM7915MZT model, 20–200x magnification, 5 MPx camera and *DinoCapture v2.0* software).

Dynamic properties: On the cubic specimens, the ultrasonic propagation velocity of the P-waves (Vp) was determined (UNE-EN 14579:2005 (39)). The equipment used was a *PROCEQ Pundit Lab+* (transducers: 54 kHz frequency, 5 cm diameter). The different anisotropies (dM-dm) of this sandstone were also calculated from the Vp values (40-42).

Structural and hydric properties: Mercury intrusion porosimetry (MIP) was used to determine pore structure (percentage, size and shape of the pores, and their distribution) (ASTM D4404:2010 (43)). Four cylindrical specimens (1.2 x 2 cm) were cut and a *Micromeritics Autopore IV 9500* porosimeter was used. In order to determine the hydric behaviour of this sandstone, the following hydric tests were carried out: 1) the cubic specimens were subjected to saturation (UNE-EN 1936:2007 (44)), which also determined density and water porosity, and water absorption by immersion and desorption by evaporation at atmospheric pressure (UNE-EN 13755:2008 (45) and NORMAL 7/81 (46)). 2) The prismatic specimens were subjected to water absorption by capillarity (UNE-EN 15801:2010 (47)). 3) The square plates were subjected to water vapour permeability (UNE-EN 15803:2010 (48)) using the wet tray method, which simulated high humidity conditions (93%) inside the material. In addition, air permeability was calculated on the cubic specimens using a *Tiny Perm II* measuring device and the formula [$T = - 0.8206 \cdot \log10(K) + 12.8737$], where T is the value obtained by the device and K is the air permeability in millidarcy (mD).

Mechanical properties: The Leeb surface hardness test (HLD) was performed (UNE-EN ISO 16859-1:2016 (49)) using the *PROCEQ Equotip 3* with an impact energy of 11.5 Nmm (D probe). Additionally, the Schmidt (R) surface hardness test was carried out (ASTM D5873-14:2016 (50) and ISRM (51)) using a *PROCEQ Rock Schmidt L type* digital sclerometer with an impact energy of 535 Nmm. Both tests were carried out on cubic specimens. Indirectly, the sclerometer estimated the unconfined compressive strength (UCS) using the formula of Katz *et al.* (52), [$UCS\ (MPa) = 2.208 \cdot e^{0.067R}$, with $R^2 = 0.964$], where R is the Schmidt hardness value.

2.2.3 Durability: Accelerated ageing tests

In order to determine the durability of Demanda Gold sandstone and to assess the effectiveness of the conservation treatment applied, this lithological variety was subjected to a highly aggressive accelerated ageing test combining the action of both water and salts ($Na_2SO_4 \cdot 10H_2O$ at 14%) (UNE-EN 12370:2020 (53)). Thirty daily cycles of immersion in dissolved-salt water (4 h) and drying in a constant heated atmosphere at 25ºC (20 h) were carried out.

After the salt resistance test, the specimens (ADDs and ADDTs) were again characterised both petrographically and petrophysically in order to quantify the changes undergone and to estimate their quality and durability, as well as the suitability and effectiveness of the treatment applied (Table 1).

3. RESULTS AND DISCUSSION

3.1 Petrographic characterization

This lithological variety is a detrital, homogeneous, massive, light beige-colored and strongly cohesive sedimentary rock (ADD) (Figure 1). Although the treatment initially affected its visual appearance, at 50 days after application no differences were observed between treated (ADDT) and untreated (ADD) specimens. Product penetration depth in the specimens was ~5 mm. After the ageing tests (ADDs, AD-

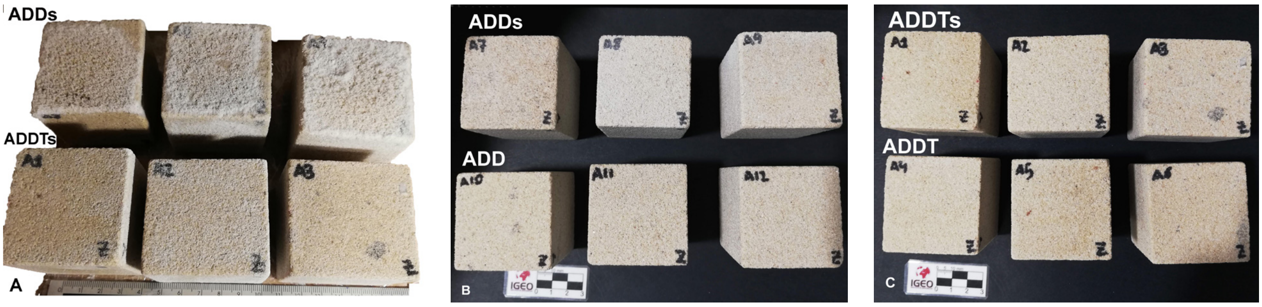

FIGURE 2: General appearance of the test specimens before and after the treatment and salt crystallisation test. A: Powdery appearance with salts on the surface, B–C: Appearance after removal of the salts from the test specimens.

DTs), the salts were detected on the surface as white powdery residues that mainly affected and lightened the color of the untreated specimens (Figure 2).

Microscopically (PLM) and mineralogically (XRD), this sandstone (ADD) is mainly formed of single-crystal subangular quartz grains (> 75%) and some polycrystalline quartz, feldspars (5– 10%), and muscovites, biotites and tourmalines (< 5%) (54). Grain size ranges from medium to coarse sand (0.25–1 mm), with a relatively good size selection. Some of the feldspars are altered to clay mineral (illite) due to geological mineral transformation processes. The single-crystal quartz grains show a significant syntaxial cement, which favours their high intergranular cohesion (Figure 3A–C). Between the grains, there is a sparse kaolinite clay matrix (< 5%) and high intergranular void porosity (> 15%), with pore sizes of up to 0.8 mm (Figure 3D). The good compositional and textural maturity of this sandstone favour its high porosity. This sandstone is classified as subarkose (55).

In the ADDT, the treatment appears as a cracked and irregular surface coating (hydrophobic layer of oligomeric polysiloxanes) up to 80 µm thick, and as a micrometric film (< 40 µm) with high optical relief surrounding the grains on the inside (silicic acid consolidating film), but without filling the intergranular porosity (Figure 3E–F). After the accelerated ageing test with salts, the ADDs shows a small increase in porosity as the clays (kaolinite and illite) partially disappear, both from the matrix and from the interior of the altered feldspars (Figure 3A–C). The salts also generate fissures that break the syntaxial cement between the quartz grains (Figure 3C–D). In the ADDTs, the aggression is more evident in the outer or superficial areas, where it breaks up the treatment film, detaching it and dispersing it in some areas (Figure 3G–H).

The presence of abundant syntaxial cement between the quartz grains is mainly responsible for both the high intergranular cohesion of this sandstone and its hardness. In addition, the existence of large pores seems to favour its resistance to salt crystallisation, as only the smaller pores are able to generate fissures (2, 5, 6, 9).

Although the FTIR technique is very effective for the detection of treatments, in this study it has been hampered because the ESTEL 1100 product has a significant siliceous component (Si-O-Si and Si-OH groups), so its vibration bands (1170, 1090, 799-780 and 450 cm^{-1}) are the same as those of quartz (Si-O). Nevertheless, the treatment could be identified by the presence of the C- H alkane groups of the water repellent (CH2-CH3: 2990 single peak and 1450-1380 cm^{-1} double peak).

3.2 Petrophysical characterisation

Surface properties: Aesthetically, ADD is a light yellowish-grey luminous sandstone with a high lightness value ($L^* = 71.5$) and yellowness index (YI = ~25) and a low chroma value ($C^* < 14$), albeit with yellow tonality ($b^* = 13.2$) (Table 2). The treatment causes a slight darkening of the specimens (ADDT) and slightly intensifies their yellow tonality ($L^* = 62.2$, $C^* = 18$, $b^* > 17$ and YI > 34). At 50 days after treatment (ADDT), these values tend to be similar to the original values. After deterioration with salts (ADDs), specimens gain lightness ($L^* > 74$) but lose colour ($C^* = 11.5$), becoming lighter due to the appearance of salts on their surface. Conversely, salts hardly affect the treated specimens (ADDTs), which present similar colour parameters to the ADDT-3 and are practically the same as the original untreated specimens (Table 2). The colour difference (ΔE^*; Table 3) shows that in the first month the treatment modified the original colour of the sandstone ($\Delta E^* = 10.3$) significantly enough for it to be detectable to the eye ($\Delta E^* > 5$) (56, 57). At 50 days after treatment, these differences decreased ($\Delta E^* = 4.1$) and were no longer visible. With the presence of salts, the ΔE^* was minimal, especially with respect to the initially treated sandstone ($\Delta E^* = 1.7$), confirming that the visual effect was negligible. Gloss and its variations are low (1.2–1.6 UB at 60° and 0.5–0.7 UB at 85°) and very constant, despite treatment and salt aggression. Values < 10 UB establish that this sandstone is matt (36). ESTEL 1100 does not cause relevant aesthetic modifications in either this type of sandstone or in others with similar chromatic parameters (25).

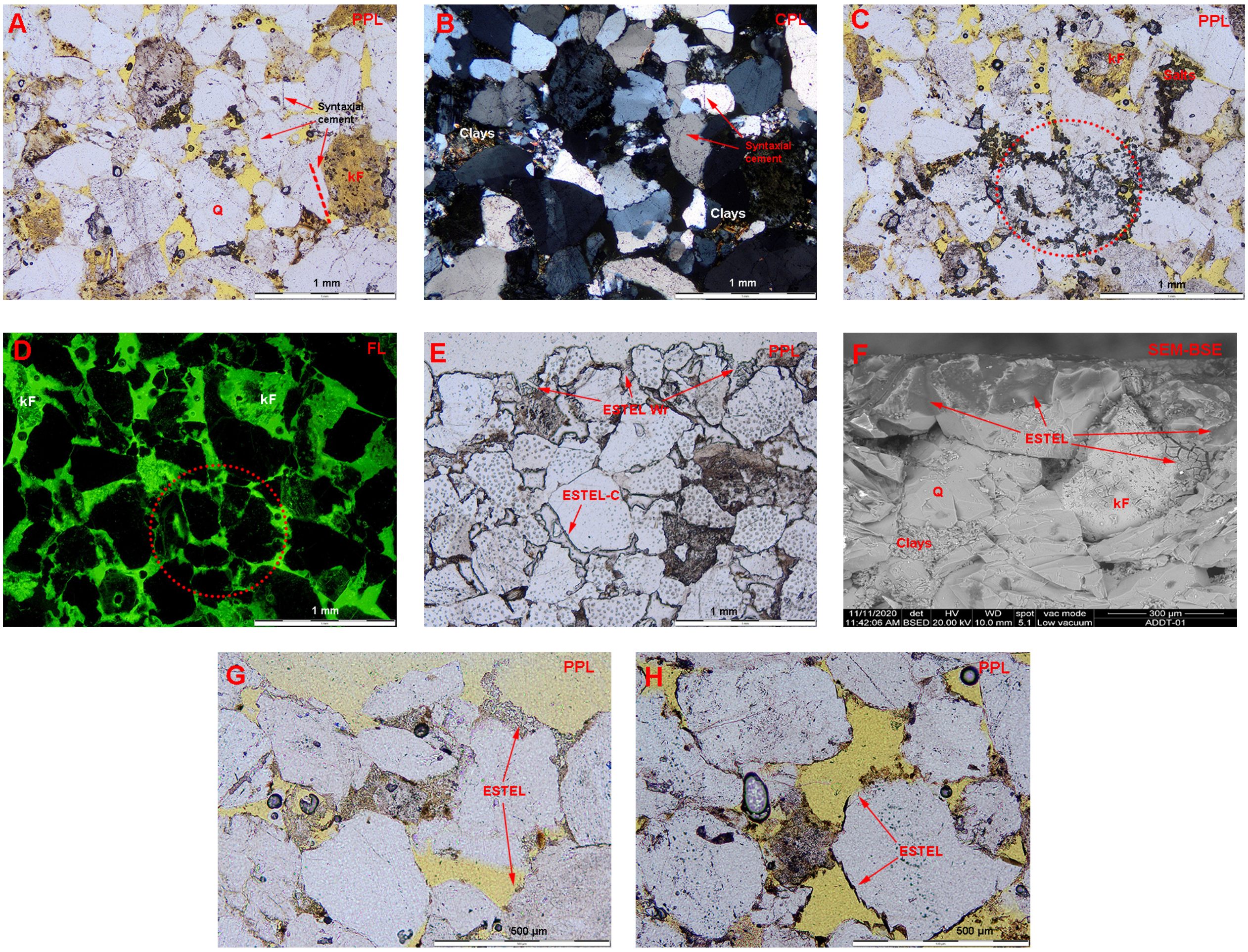

FIGURE 3. Images under different types of optical microscope: parallel (PLL: A, C, E, G, H) and crossed (CPL: B) polarised light; fluorescent light (FL: D); and scanning electron microscopy in backscattered electron mode (SEM-BSE: F). **A–B**: (ADD), Dominant mineralogy (quartz [Q], potassium feldspar [kF]), with feldspars transformed into clays or with porosity because of the lack of clay, and with quartz syntaxial cement binding the quartz grains. **C–D**: (ADDs), show abundant porosity (yellow pores [C] and green pores [D]), and how salts break the syntaxial cement (circle). **E–F**: (ADDT), the ESTEL 1100 treatment appears as a fissured water-repellent layer (ESTEL [Wr]) on the surface and as a dense film (ESTEL [C]) surrounding the grains. **G– H: (**ADDTs), Salts breaking up and detaching the treatment, which appears irregularly.

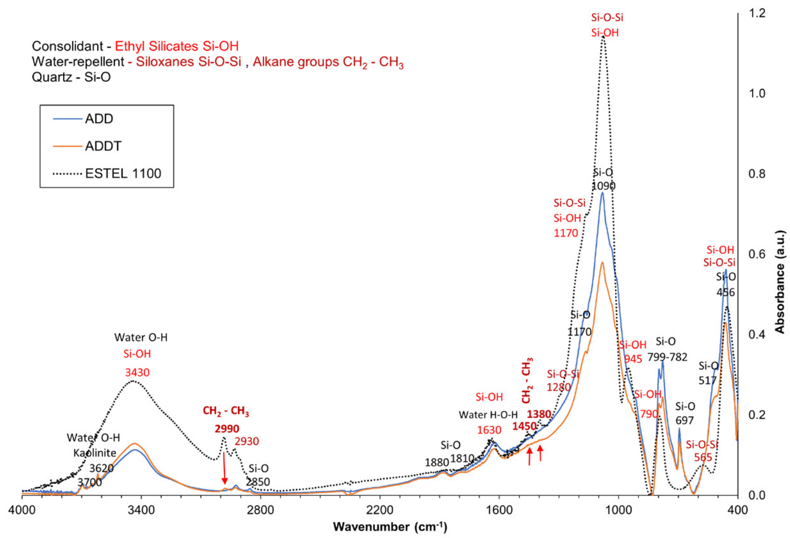

FIGURE 4. FTIR spectra for the untreated (ADD) and treated (ADDT) sandstones, and for the ESTEL1100.

Table 2. Average chromatic parameter values: lightness (L*), red/green (a*), blue/yellow (b*), chroma (C*), whiteness index (WI) and yellowness index (YI). (2): At 29 days after treatment. (3): At 50 days after treatment. (4): At 118 days after treatment and salts.

	ADD	ADDs	ADDT (2)	ADDT (3)	ADDTs (4)
L*	71.5 ± 0.1	74.2 ± 1.3	62.2 ± 0.4	67.7 ± 0.4	69.2 ± 0.1
a*	3.5 ± 0.1	3.1 ± 0.3	5.1 ± 0.3	4.0 ± 0.2	3.7 ± 0.0
b*	13.2 ± 0.3	11.1 ± 0.8	17.1 ± 0.4	14.3 ± 0.5	13.7 ± 0.5
C*	13.7 ± 0.3	11.5 ± 0.9	17.8 ± 0.4	14.9 ± 0.5	14.2 ± 0.5
WI	0.7 ± 0.9	9.3 ± 3.6	-11.6 ± 0.8	-3.9 ± 1.3	-1.6 ± 1.4
YI	24.7 ± 0.5	20.5 ± 1.7	34.3 ± 0.8	27.6 ± 0.9	26.1 ± 0.9

Table 3. Chromatic variations (ΔE*) between the different specimens. (2): At 29 days after treatment. (3): At 50 days after treatment. (4): At 118 days after treatment and salts.

	ΔE*
ADD vs ADDT (2)	10.3
ADD vs ADDT (3)	4.1
ADD vs ADDs	3.4
ADDT (3) vs ADDTs (4)	1.7
ADD vs ADDTs (4)	2.4

The static contact angle between a water droplet and the surface of this sandstone establishes its strong hydrophilic character, producing similar results both before (θADD = 29° ± 5.2°) and after (θADDs = 32.7° ± 7.2°) ageing tests. The treatment makes it hydrophobic (θADDT > 106° ± 6.8°) until after the attack with salts, which returns it to its initial hydrophilic state, albeit with a greater contact angle (θADDTs > 56° ± 8.3°) due to the cracking and partial dispersal of the hydrophobic agent on the surface (Figure 5). Infrared thermography has determined that the treated specimens, both before (ADDT) and after the aggression with salts (ADDTs), tend to retain heat for longer. After a cycle of heating to 55 °C followed by 30 min of cooling, the difference between the treated and untreated sandstones was +3–4 °C. The application of ESTEL 1100 to the surface of this sandstone therefore seems to favour the retention of the heat absorbed from the outside for longer, reducing the material's thermal conductivity.

Dynamic properties: These porous sandstones' high intergranular cohesion, due to the natural syntaxial cement around the dominant quartz grains, results in high P-wave propagation velocities (VpADD ~2667 m/s). These values are similar to the averages of quartz-rich sandstones (quartz arenites-subarkoses) with crystalline cement (2, 3, 9). The treatment led to a considerable increase on their original values (VpADDT ~3832 m/s) (Table 4). After deterioration with salts, the Vp of the ADDs increased slightly (by ~150 m/s), possibly because of the presence of crystallised salts inside its pores (58). However, the Vp of the ADDTs decreased by up to 345 m/s because of breakup and dispersal of the surface treatment. In addition, this sandstone exhibits low anisotropy (dMm ADD ~19%, dM ADD < 12%, (40)), although it does have a preferential anisotropy orientation (dM > dm; Table 4), possibly related to the bedding planes typical of sandstones and which in this case are not visible at the macroscopic level. The treatment lowers and homogenises its initial anisotropy (dMmADDT = 11.5%), making its preferred direction practically disappear, especially after salt crystallisation (dM ADDTs~dm ADDTs). There is a linear correlation between propagation velocity (Vp) and total anisotropy (dM) that results in a substantial difference between treated and untreated sandstones. While the original sandstones with (ADDs) and without salts (ADD) on average show lower Vp (2600–2800 m/s) and higher total anisotropy (dM = 8–14), the treated (ADDT) and ageing (ADDTs) sandstones show higher Vp (> 3400 m/s; a 30% increase) and lower anisotropy (dM = 6–8; a decrease of up to 40%).

Table 4. Average P-wave propagation velocity (Vp) and anisotropy values: total (dM), relative (dm) and complete (dMm (40)).

	Vp (m/s)	dM (%)	dm (%)	dMm (%)
ADD	2667 ± 53	11.79 ± 2.3	7.24 ± 2.1	19.03 ± 4.1
ADDs	2811 ± 66	8.83 ± 1.1	3.88 ± 1.4	12.70 ± 2.4
ADDT	3832 ± 53	7.03 ± 0.9	4.43 ± 1.1	11.47 ± 1.1
ADDTs	3487 ± 85	7.50 ± 1.9	6.32 ± 1.7	13.81 ± 0.6
WI	0.7 ± 0.9	9.3 ± 3.6	-11.6 ± 0.8	-3.9 ± 1.3
YI	24.7 ± 0.5	20.5 ± 1.7	34.3 ± 0.8	27.6 ± 0.9

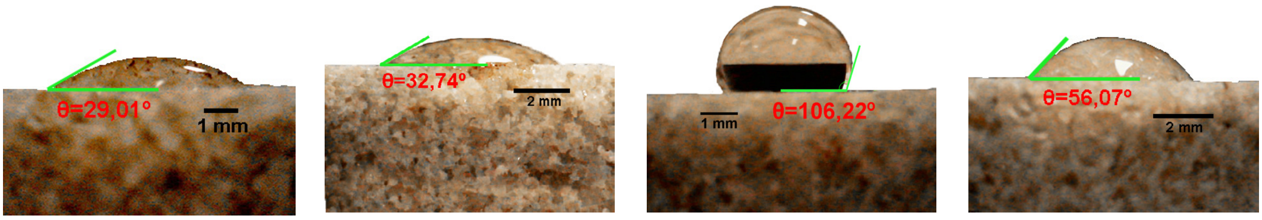

Figure 5. Changes in static contact angle for ADD, ADDs, ADDT and ADDTs.

Table 5. Average values of the main structural and hydric properties.

		ADD	ADDs	ADDT	ADDTs
	Real density, ρ_r (kg/m^3)	2641 ± 0.7	2637 ± 0.9	2588 ± 3.5	2604 ± 1.0
	Bulk density, ρ_{ap} (kg/m^3)	2148 ± 8.0	2148 ± 9.2	2184 ± 5.2	2175 ± 5.8
	Total porosity (%)	18.83 ± 0.3	18.7 ± 0.4	15.75 ± 0.2	16.62 ± 0.2
Geometry	**Specific pore surface area (m^2/g)**	0.26	0.22	0.29	0.17
	Average pore diameter (µm)	1.2	1.14	0.6	1.14
	Average pore size (µm)	10.4	16.9	14.5	16.1
	Pore size distribution (%)	Micro: 29.0 Macro: 71.0	Micro: 34.2 Macro: 65.8	Micro: 28.9 Macro: 71.1	Micro: 30.7 Macro: 69.3
	Tortuosity	10.1	6.59	18.2	2.37
	Compactness index (0-1)	0.81	0.81	0.84	0.83
	Saturation (%)	8.69 ± 0.2	8.63 ± 0.2	7.13 ± 0.1	7.57 ± 0.1
	Water absorption coefficient at Patm (%)	5.52 ± 0.1	5.33 ± 0.1	1.11 ± 0.1	1.76 ± 0.1
	Capillary absorption coefficient (kg/m^2·s^{0,5})	$0.03308 \pm 2.23 \cdot 10^{-3}$	$0.03208 \pm 1.61 \cdot 10^{-3}$	$0.002598 \pm 7.53 \cdot 10^{-6}$	$0.002875 \pm 2{,}1 \cdot 10^{-4}$
	Water vapour permeability coefficient (kg/m·s·Pa)	$1.63 \cdot 10^{-9} \pm 3.7 \cdot 10^{-11}$	$2.97 \cdot 10^{-9} \pm 1.1 \cdot 10^{-10}$	$1.14 \cdot 10^{-9} \pm 1.5 \cdot 10^{-10}$	$2.73 \cdot 10^{-9} \pm 6.9 \cdot 10^{-10}$
	Air permeability (mD)	772.53 ± 326.2	484.15 ± 50.4	315.98 ± 40.6	380.75 ± 74.7

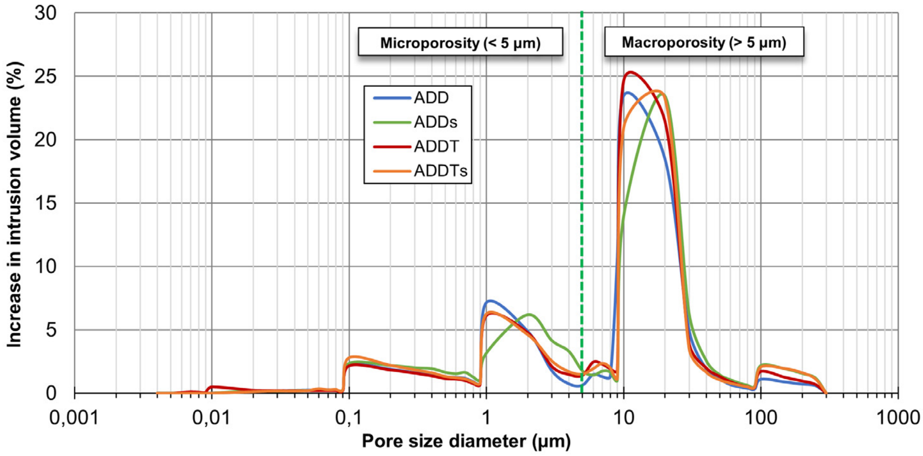

Figure 6. Pore size distribution curves for ADD, ADDs, ADDT and ADDTs.

Structural and hydric properties: Untreated sandstone (ADD) has a high real density (~2640 kg/m^3) due to its high quartz composition (2, 3). The difference with the average bulk density (~2150 kg/m^3) reflects its high porosity of almost 19%, with 99% being open porosity (Table 5). Its pore system is determined by the monomodal distribution (10–30 µm) of the dominant macroporosity (71%; Figure 6). Average pore size is 10.4 µm and pore geometry tends to be regular and equidimensional with a specific surface area of 0.26 m^2/g and a pore diameter of 1.2 µm. With this porosity, this sandstone saturates at 8.7 wt% and has an average 48 h water absorption coefficient of 5.5 wt% and total absorption of 6.6 wt%, being able to absorb 78% of this total in the first 2 minutes. Similarly, it loses 75% of the absorbed water in only 24 h, not retaining any water internally (Table 5, Figure 7). Capillary water absorption is ~14 kg/m^2, with 73% absorbed in the first 3–4 h. This implies a high capillary absorption coefficient (~0.0331 kg/m^2·s$^{0.5}$; Table 5, Figure 8). These sandstones also exhibit high permeability values, both to water vapour (~$1.6 \cdot 10^{-9}$ kg/m·s·Pa) and air (~772.5 mD) (Table 5). All these structural and physical values are similar to those described for quartz arenites and subarkoses from different geological ages (2-4, 9, 59).

Application of ESTEL 1100 reduces porosity in this sandstone to 15.7% without causing any changes in its modal distribution or its micro/macroporosity ra-

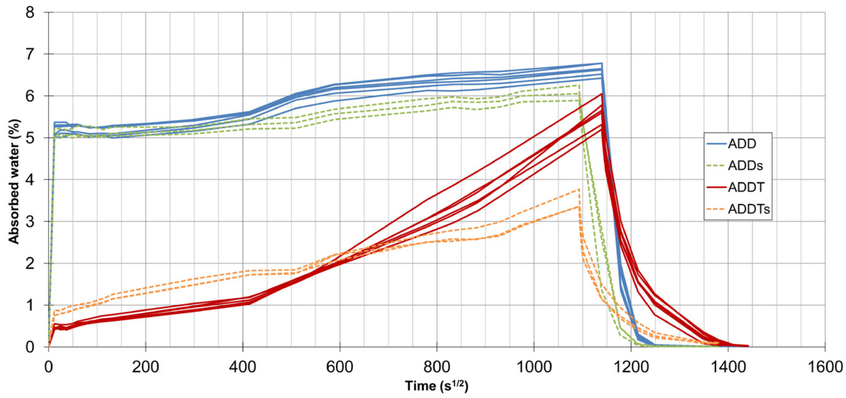

FIGURE 7. Kinetic behaviour of free water absorption and desorption for ADD, ADDs, ADDT and ADDTs.

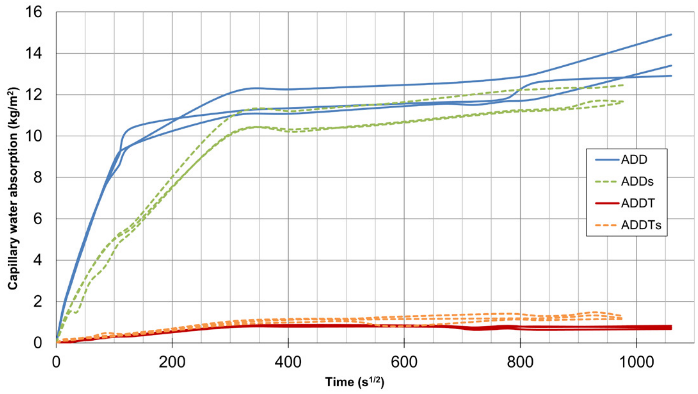

FIGURE 8. Capillary water absorption curves for ADD, ADDs, ADDT and ADDTs.

tio (Table 5; Figure 6). Average pore size increases to 14.5 µm and pore geometry becomes more irregular, reducing pore diameter (0.6 µm) and increasing specific surface area (0.29 m^2/g). Also, capillary connections become more sinuous (tortuosity = 18.2), which restricts the mobility of water inside the sandstone and reduces the degree of saturation (~7 %; Table 5). These pore geometry changes substantially modified the sandstone's behaviour and absorption capacity (Figure 7). Water absorption takes place slowly and progressively, presenting a low absorption coefficient at 48 h (1.1 wt%) but a total absorption capacity (5.6 wt%) similar to that of untreated sandstone. Similarly, the outflow of water from the interior is also restricted, with 52% of the total water absorbed evaporating in 24 h and 3% being retained internally. The treatment also significantly reduces (90%) the water absorbed by capillary action (< 1 kg/m^2), saturating in less than 24 h and presenting a very low capillary absorption coefficient (~0.0026 $kg/m^2 \cdot s^{0.5}$; Table 5, Figure 8). The negative influence of the treatment on the internal mobility of water vapour and air, which affects the respective permeabilities, is also noteworthy (Table 5). While vapour permeability is reduced by one third (~$1.14 \cdot 10^{-9}$ kg/m·s·Pa), air permeability is reduced by up to 60% (~316 mD) (Table 5). ESTEL 1100 effectively restricts the ingress of water in this sandstone, but it also restricts its egress by reducing transpiration, which may affect the durability of this material (25, 27, 60).

Salt aggression does not cause significant changes to the structural and hydric properties of the original sandstone (ADD and ADDT; Table 5, Figure 6–8). The most important changes are related to the increase in average pore size, which in both cases (ADDs and ADDTs) exceeds 16 µm, possibly because of the removal of the few clays they contain. Also, microporosity increases slightly (> 30%) to the detriment of macroporosity, which remains dominant (60). The geometry of the pores (0.22-0.17 m^2/g and 1.14 µm) and their capillary connections (tortuosity = 6.6–2.4) become more regular and straighter, establishing a new fissure microporosity — especially in the treated sandstones (ADDTs) — detected by PLM and FLM. This means that the capacity of the ADDTs to absorb embedded and capillary water is greater than that of the ADDs, where the possible presence of salts may have hindered water ingress. The ADDTs also has a higher water absorption coefficient (~1.8 wt%) than ADDT, although its total absorption is lower (3.5 wt%; Table 5, Figure 7). Capillary water absorption after salt aggression evolves in the same direction as in the ADD and ADDT (Figure 8). While in the ADDs these values are somewhat lower (~12 kg/m^2; ~0.0321 $kg/m^2 \cdot s^{0.5}$)

and the sandstone takes 24 h to absorb > 85% of its total capacity, in the ADDTs this value rises slightly (~1.2 kg/m^2; ~0.0029 $kg/m^2 \cdot s^{0.5}$), favoured by treatment breakup and better water mobility (Table 5; Figure 8). Air permeability follows the same behaviour. In the ADDTs it rises by 17% (~380 mD) because the treatment breaks up, but in the non-treated samples it falls to 35% (~484 mD) because salts fill its pores, restricting air movement (Table 5). In contrast, the salts significantly affect initial water vapour permeability almost equally, doubling it in each case (Table 5). Salt crystallisation near the surface would favour an increase in these sandstones' water vapour permeability because of the increase in microporosity (31–34%) after aggression in both the treated and untreated specimens. The fact that these sandstones show a large pore size domain (> 10 µm) makes them less susceptible to degradation by the effect of crystallisation of salts that exert high crystallisation pressure, such as mirabilite ($Na_2SO_4 \cdot 10H_2O$) (9, 15, 19, 20).

Mechanical properties: The Demanda Gold sandstone shows high surface hardness and strength (~427 HLD, ~48 RL and > 55 MPa) (51, 52, 61-64) due to the quartz grains and associated quartz syntaxial cement, which are directly responsible for its cohesion (Table 6). However, such hardness could have been even greater if it were not for the high porosity of this sandstone. The strong correlation between composition and hardness concurs with other authors' (62-64) findings for similar sandstones. The partial coating of the sandstone's pores with the ESTEL 1100 treatment does not affect Leeb surface hardness, but it does affect Schmidt hardness and unconfined compressive strength, which are substantially improved (52 RL, > 72 MPa) (25, 51, 52). The presence of salts in surface porosity after aggression (ADDs and ADDTs) reduces Leeb surface hardness as it can have an impact at single-mineral level on soft (salts) or weakened (feldspars) grains or crystals (364–382 HLD). However, on a larger scale, salt aggression does not modify either Schmidt hardness (~48 RL) or UCS (~55 MPa) in the untreated sandstone (ADDs), but it does modify them in treated sandstones (ADDTs), where both parameters are reduced (> 50 RL, > 64 MPa), thus lowering their hardness and strength. Moreover, the filling of this porosity by both the treatment and the salts makes the resistance to external stress homogeneous in its three spatial directions, eliminating the preferential anisotropy orientation that the sandstones originally showed (ADD) and that was detected in previous tests (Vp and dM).

Table 6. Average superficial hardness (HLD, RL) and unconfined compressive strength (UCS) values.

	ADD	ADDs	ADDT	ADDTs
Leeb hardness (HLD)	426.7 ± 25.3	382.3 ± 5.8	422.2 ± 55.8	363.8 ± 32.6
Schmidt hardness (RL)	47.92 ± 2.8	47.67 ± 2.8	52.00 ± 1.9	50.33 ± 1.5
UCS (MPa)	55.58 ± 11.8	54.67 ± 10.8	72.58 ± 9.9	64.67 ± 6.5

4. CONCLUSIONS

Demanda Gold sandstone is a Cretaceous subarkose with good compositional and textural maturity that determine its petrographic and petrophysical properties. These intrinsic properties make this sandstone an outstanding building material. Moreover, its response to the weathering and salt crystallisation tests would seem to confirm its durability. The dominant monomineralic composition (quartz grains), the high-strength cement and the high monomodal porosity (~19%) determine its physical and mechanical properties. Its mineralogy makes it a dense material (> 2600 kg/m^3) with high ultrasonic propagation velocities (2660 m/s) and high hardness (~48 RL, > 55 MPa). Because of its dominant macroporosity (71% measuring 10–30 µm) it has high water absorption (embedded and capillary) and air and water vapour permeability coefficients.

Application of the ESTEL 1100 treatment effectively fulfils a dual function, cementing (consolidating) up to a depth of ~5 mm and waterproofing (water-repellent) on the surface, substantially improving the sandstone's physical-mechanical properties. Although the sandstone's original porosity is only reduced to 16–17%, the treatment does significantly modify the geometry of its pores and capillary connections, making them more irregular and sinuous. Not only does this restrict water, water vapour, air and even heat ingress and mobility inside the stone, it also hinders their egress. This results in reductions of 80–90% in water absorption capacity (embedded and capillary), of 60% in air permeability and of 30–35% in water vapour permeability. Similarly, the treatment does not significantly modify the sandstone's aesthetic appearance as it does not change its chromatic parameters or its gloss, although it does reduce its original anisotropy. It also increases its ultrasonic propagation velocity by almost 30% (3800 m/s), its surface hardness by ~8% (52 RL) and its UCS by > 23% (> 72 MPa). In conclusion, the treatment improves the quality of the stone by making it harder and less absorbent, although it may leave a certain amount of water retained inside (3%), which can influence its durability.

The accelerated ageing test with $Na_2SO_4 \cdot 10H_2O$ confirms these sandstones' low susceptibility to degradation by the effects of crystallisation of this salt inside their pore system. The large pore size (> 10 µm) seems to be able to contain the high crystallisation pressure of this type of salt so that the physical-mechanical variations suffered by this sandstone are minimal and non-significant. It should be noted that the presence of salts on its surface seems to have generated microporosity to the detriment of the macroporosity it fills, thus doubling its permeability to water vapour. The salts affect the treated sandstone by causing significant changes in the geometry and connectivity of its pores, which have been previously modified by the treatment and which, in this case, makes them more regular and straighter. Here, the salts break up and detach part of the surface treatment, increasing the sandstone's porosity somewhat (5%) and generating fissural microporosity that increases its water absorption capacity (embedded ~37% and capillary ~10%), which was strongly reduced after the treatment. Another consequence of this action was a reduction in its mechanical properties (of 3.2% in surface hardness and ~11% in UCS). Thus, the amount, size, modal distribution and geometry of the pores of this sandstone seem to significantly influence its resistance to weathering, improving its durability.

ACKNOWLEDGEMENTS

This work was funded under the Region of Madrid's TOP-HERITAGE-(Technologies in Heritage Science (S2018/NMT-4372) project. The authors are members of Complutense University of Madrid research team n.921349. The authors wish to acknowledge professional support of the Interdisciplinary Thematic Platform from CSIC Open Heritage: Research and Society (PTI- PAIS).

Declaration of Competing Interest. The authors declare that they have no known competing financial interests or personal relationships that could have appeared to influence the work reported in this paper.

AUTHOR CONTRIBUTIONS:

Conceptualization: M.J. Varas-Muriel. Data curation: A. Gómez Marfil. Formal analysis: M.J. Varas-Muriel, A. Gómez Marfil. Funding acquisition: M.J. Varas-Muriel. Investigation: A. Gómez Marfil. Methodology: A. Gómez Marfil. Project administration: M.J. Varas-Muriel. Resources: M.J. Varas-Muriel. Software: A. Gómez Marfil. Supervision: M.J. Varas-Muriel. Validation: M.J. Varas-Muriel, A. Gómez Marfil. Visualization: A. Gómez Marfil. Writing, original draft: M.J. Varas-Muriel, A. Gómez Marfil. Writing, review & editing: A. Gómez Marfil.

REFERENCES

1. Hosein-Ghobadi, M.; Babazadeh, R.; Khodabakhsh, S. (2014) Petrophysical and durability tests on sandstones for the evaluation of their quality as building stones using Analytical Hierarchy Process (AHP). *J. Geope*. 4 [1], 25-43. https://doi.org/10.22059/JGEOPE.2014.51190.
2. Stück, H.; Koch, R.; Siegesmund, S. (2013) Petrographical and petrophysical properties of sandstones: statistical analysis as an approach to predict material behaviour and construction suitability. *Environ. Earth Sci*. 69, 1299-1332. https://doi.org/10.1007/s12665-012-2008-1.
3. Vázquez, P.; Alonso, F.J.; Carrizo, L.; Molina, E.; Cultrone, G.; Blanco, M.; Zamora, I. (2013) Evaluation of the petrophysical properties of sedimentary building stones in order to establish quality criteria. *Const. Build. Mat.* 41, 868–878. https://doi.org/10.1016/j.conbuildmat.2012.12.026.
4. Cultrone. G.; Luque, A.; Sebastián, E. (2012) Petrophysical and durability tests on sedimentary stones to evaluate their quality as building materials. *Quart. J. Eng. Geol. Hydrog*. 45, 415-422. https://doi.org/10.1144/qjegh2012-007.
5. Ruedrich, J.; Bartelsen, T.; Dohrmann, R.; Siegesmund, S. (2011) Moisture expansion as a deterioration factor for sandstone used in buildings. *Environ. Earth Sci.* 63, 1545-1564. https://doi.org/10.1007/s12665-010-0767-0.
6. Buj, O.; Gisbert, J. (2007) Petrophysical characterization of three commercial varieties of Miocene sandstones from the Ebro valley. *Mater. Construcc.* 57 [287], 63–74. https://doi.org/10.3989/mc.2007.v57.i287.57.
7. McCabe, S.; Smith, B.J.; Warke, P.A. (2007) Preliminary observations on the impact of complex stress histories on sandstone response to salt weathering: laboratory simulations of process combinations. *Environ. Geol.* 52, 251-258. https://doi.org/10.1007/s00254-006-0531-7.
8. Forestieri, G.; Álvarez de Buergo, M. (2019) Petrophysical-mechanical behavior of Grisolia Stone found in the architectural heritage of southern Italy. *Mater. Construcc*. 69 [334], e188. https://doi.org/10.3989/mc.2019.04118.
9. Molina, E.; Cultrone, G.; Sebastián E.; Alonso, F.J. (2013) Evaluation of stone durability using a combination of ultrasound, mechanical and accelerated aging tests. *J. Geophys. Eng.* 10 [3], 035003. https://doi.org/10.1088/1742-2132/10/3/035003.
10. Esbert, R.M.; Alonso, F.J.; Ordaz. J. (2008) La petrofísica en la interpretación del deterioro y la conservación de la piedra de edificación. *Trabajos de Geología*. 28, 87-95. Univ. Oviedo.
11. Varas, M.J.; Molina, E.; Vicente, M.A. (2003) Petrophysical characteristics of the sandstones used in the construction of the Monumental Heritage of Ciudad Rodrigo, Salamanca, España. *Mater. Construcc.* 53 [269], 73-88. https://doi.org/10.3989/mc.2003.v53.i269.269.
12. Varas, M.J.; Molina, E.; Vicente, M.A. (2002) Ornamental sandstones used in Ciudad Rodrigo, Salamanca: petrographic and chemical characterization of the quarry materials. *Mater. Construcc*. 52 [266], 33-53. https://doi.org/10.3989/mc.2002.v52.i266.333.
13. García-Talegón, J.; Iñigo, A.C.; Alonso-Gavilán, G.; Vicente-Tavera. S. (2014) Villamayor Stone (Golden Stone) as a Global Heritage Stone Resource from Salamanca (NW of Spain). In: Global Heritage Stone: Towards International Recognition of Building and Ornamental Stones. Pereira, D., Marker, B. R., Kramar, S., Cooper, B. J. & Schouenborg, B. E. (eds). *Geol. Soc. London, Special Publications*. 407, 12p. https://doi.org/10.1144/SP407.19.
14. Molina, E.; Cultrone, G.; Sebastián, E.; Alonso, F.J.; Carrizo, L.; Gisbert, J.; Buj, O. (2011) The pore system of sedimentary rocks as a key factor in the durability of buildings materials. *Eng. Geol.* 118 [3-4], 110-121. https://doi.org/10.1016/j.enggeo.2011.01.008.
15. Benavente, D.; Cueto, N.; Martínez-Martínez, J.; García del Cura, M.A.; Cañaveras. J.C. (2007) The influence of petrophysical properties on the salt weathering of porous building rocks. *Environ. Geol.* 52, 215–224. https://doi.org/10.1007/s00254-006-0475-y.
16. Benavente, D.; García del Cura, M.A.; Fort, R., Ordóñez, S. (2004) Durability estimation of porous building stones from pore structure and strength. *Eng. Geol*. 74 [1-2], 113-127. https://doi.org/10.1016/j.enggeo.2004.03.005.
17. Fort, R.; Feijoo, J.; Varas-Muriel, M.J.; Navacerrada, M.A.; Barbero-Barrera, M.M.; De la Prida, D. (2022) Appraisal of non-destructive in situ techniques to determine moisture - and salt crystallization- induced damage in dolostones. *J. Build. Eng.* 53, 104525. https://doi.org/10.1016/j.jobe.2022.104525.
18. Angeli, M.; Bigas, J.P.; Benavente, D.; Menéndez, B.; Hébert R.; David, C. (2007) Salt crystallization in pores: quantification and estimation of damage. *Environ. Geol.* 52, 205–213. https://doi.org/10.1007/s00254-006-0474-z.

19. Ruedrich J.; Siegesmund, S. (2007) Salt and ice crystallisation in porous sandstones. *Environ. Geol.* 52, 225–249. https://doi.org/10.1007/s00254-006-0585-6.
20. Benavente, D.; García del Cura, M.A.; García-Guinea, J.; Sánchez-Moral, S.; Ordoñez, S. (2004) Role of pore structure in salt crystallisation in unsaturated porous stone. *J. Crys. Growth*. 260, 532-544. https://doi.org/10.1016/j.jcrysgro.2003.09.004.
21. Varas-Muriel, M.J.; Pérez-Monserrat, E.M.; Vázquez-Calvo, M.C.; Fort, R. (2015) Effect of conservation treatments on heritage stone. Characterisation of decay processes in a case study. *Const. Build. Mat.* 95, 611-622. https://doi.org/10.1016/j.conbuildmat.2015.07.087.
22. Varas-Muriel, M.J.; Alvarez de Buergo, M.; Fort, R. (2007) The influence of past protective treatments on the deterioration of historic stone façades: A case study. *Stud. Conser*. 52 [2], 110-124. https://doi.org/10.1179/sic.2007.52.2.110.
23. Esbert, R.M.; Díaz Pache, F. (1993) Influencia de las características petrofísicas en la penetración de consolidantes en rocas monumentales porosas. *Mater. Construcc*. 43 [230], 25-36.
24. Pozo-Antonio, J.S.; Noya, D.; Montojo, C. (2020) Aesthetic effects on granite of adding nanoparticle TiO2 to Si-Based consolidants (ethyl silicate or nano-sized silica). *Coatings*. 10 [3], 215. https://doi.org/10.3390/coatings10030215.
25. Luque, A.; Cultrone, G.; Sebastián, E.; Cazalla, O. (2008) Effectiveness of stone treatments in enhancing the durability of bioclastic calcarenite (Granada, Spain). *Mater. Construcc.* 58 [292], 115-128. https://doi.org/10.3989/mc.2008.41607.
26. Zendri, E.; Biscontin, G.; Nardini, I.; Riato, S. (2007) Characterization and reactivity of silicatic consolidants, *Const. Buil. Mat.* 21 [5], 1098-1106. https://doi.org/10.1016/j.conbuildmat.2006.01.006.
27. Fort, R.; Álvarez de Buergo, M.; Varas-Muriel, M. J.; Vázquez-Calvo, M.C. (2005) Valoración de tratamientos con polímeros sintéticos para la conservación de materiales pétreos del patrimonio. *R. Plásticos Modernos.* 89 [583], 83-89.
28. Mas, R.; García, A.; Salas, R.; Meléndez, A.; Alonso, A.; Aurell, M.; Bádenas, B.; Benito, M.I.; Carenas, B.; García-Hidalgo, J.F.; Gil, J.; Segura, M. (2004) Segunda fase de rifting: Jurásico Superior-Cretácico inferior. In: Vera, J. A. (ed.) Geología de España, IGME, SGE. 503- 522.
29. Arribas, J.; Ochoa, M.; Mas, R.; Arribas, Mª. E.; González-Acebrón, L. (2007) Sandstone petrofacies in the northwestern sector of the Iberian Basin. *J. Iberian Geol.* 33 [2], 191-206.
30. SIEMCALSA (Sociedad de Investigación y explotación Minera de Castilla y León) (2008) La piedra natural en Castilla y León. Junta de Castilla y León. Consejo de Economía y Empleo. Domènech e-learning multimedia, S.A. ediciones. Deposito Legal: B-3721-2008.
31. UNE-EN 16515 (2016) Conservación del patrimonio cultural. Métodos de ensayo. Líneas directrices para caracterizar la piedra natural utilizada en el patrimonio cultural. Asociación Española de Normalización y Certificación (AENOR). Madrid.
32. UNE-EN 12407 (2020) Métodos de ensayo para la piedra natural. Estudio petrográfico. Asociación Española de Normalización y Certificación (AENOR). Madrid.
33. Varas-Muriel, M.J. (2012) Técnicas de caracterización petrológicas (II): microscopía óptica de fluorescencia (MOF) y microscopía electrónica de barrido (MEB). En: La conservación de los geomateriales utilizados en el patrimonio. Ed. Programa Geomateriales. Comunidad de Madrid. España, pp. 31-36. ISBN: 978-84-615-7660-9.
34. UNE-EN 15886 (2011) Conservación del patrimonio cultural. Métodos de ensayo. Medición del color de superficies. Asociación Española de Normalización y Certificación (AENOR). Madrid.
35. ASTM E313 (2020). Standard practice for calculating yellowness and whiteness indices from instrumentally measured color coordinates. American Society for Testing and Materials (ASTM). West Conshohocken, PA, 19428-2959. Unites States. https://doi.org/10.1520/E0313-20.
36. ASTM D523-14 (2018) Standard test method for specular gloss. American Society for Testing and Materials (ASTM). Pennsylvania, 2018. https://doi.org/10.1520/D0523-14.
37. UNE-EN 16714 (2017) Ensayos no destructivos. Ensayo por termografía. Asociación Española de Normalización y Certificación (AENOR). Madrid.
38. UNE-EN 15802 (2010) Conservación del patrimonio cultural. Métodos de ensayo. Determinación del ángulo de contacto estático. Asociación Española de Normalización y Certificación (AENOR). Madrid.
39. UNE-EN 14579 (2005) Métodos de ensayo de piedra natural. Determinación de la velocidad de propagación del sonido. Asociación Española de Normalización y Certificación (AENOR). Madrid.
40. Fort, R.; Varas, M.J.; Álvarez de Buergo, M.; Freire-Lista, D.M. (2011) Determination of anisotropy to enhance the durability of natural stone. *J. Geophys. Eng.* 8 [3], 132-144. https://doi.org/10.1088/1742-2132/8/3/S13.
41. Fort, R.; Fernández-Revuelta, B.; Varas, M. J.; Álvarez de Buergo, M.; Taborda-Duarte, M. (2008) Influence of anisotropy on the durability of Madrid-region Cretaceous dolostone exposed to salt crystallization processes. *Mater. Construcc.* 58, 289-290. https://doi.org/10.3989/mc.2008.v58.i289-290.74.
42. Guyader, J.; Denis, A. (1986) Propagation des ondes dans les roches anisotropes sous contrainte évaluation de la qualité des schistes ardoisiers. *Bullet. Eng. Geol.* 33, 49-55. https://doi.org/10.1007/BF02594705.
43. ASTM D4404 (2010) Standard test method for determination of pore volume and pore volume distribution of soil and rock by Mercury Intrusion Porosimetry. American Society for Testing and Materials (ASTM). Pennsylvania, 2010. United States. https://doi.org/10.1520/D4404-18.
44. UNE-EN 1936 (2007) Métodos de ensayo para piedra natural: Determinación de la densidad real y aparente y de la porosidad abierta y total. Asociación Española de Normalización y Certificación (AENOR). Madrid.
45. UNE-EN 13755 (2008) Métodos de ensayo de piedra natural. Determinación de la absorción de agua a presión atmosférica. Asociación Española de Normalización y Certificación (AENOR). Madrid.
46. NORMAL 7/81 (1981) Assorimiento d'acqua per inmersione totale. Capacitá di imbibizione. Doc., CNR-ICR. Roma. 5p.
47. UNE-EN 15801 (2010) Conservación del patrimonio cultural. Métodos de ensayo. Determinación de la absorción de agua por capilaridad. Asociación Española de Normalización y Certificación (AENOR). Madrid.
48. UNE-EN 15803 (2010) Conservación del patrimonio cultural. Métodos de ensayo. Determinación de la permeabilidad al vapor de agua. Asociación Española de Normalización y Certificación (AENOR). Madrid.
49. UNE-EN ISO 16859-1 (2016) Materiales metálicos. Ensayo de dureza Leeb. Parte 1: Método de ensayo. (ISO 16859-1:2015). Asociación Española de Normalización y Certificación (AENOR). Madrid.
50. ASTM D5873-14 (2016) Standard test method for determination of rock hardness by rebound hammer method. American Society for Testing and Materials (ASTM). West Conshohocken, PA, 2000. http://doi.org/10.1520/D5873-14.
51. Aydin, A. (2009) ISRM (International Society for Rock Mechanics Commission) Suggested method for determination of the Schmidt hammer rebound hardness: revised version. *Int. J. Rock Mech. Min. Sci.* 46 [3], 627-634. https://doi.org/10.1016/j.ijrmms.2008.01.020.
52. Katz, O.; Reches, Z.; Roegiers, J.C. (2000) Evaluation of mechanical rock properties using a Schmidt Hammer. *Int. J. Rock Mech. Min. Sci.* 37 [4], 723–28. https://doi.org/10.1016/S1365-1609(00)00004-6.
53. UNE-EN 12370 (2020) Métodos de ensayo para piedra natural. Determinación de la resistencia a la cristalización de las sales. Asociación Española de Normalización y Certificación (AENOR). Madrid.
54. Baccelle, L.; Bosellini, A. (1965) Diagrammi per la stima visive della composizione percentuale nelle rocche sedimentarie. Annali dell'Università di Ferrara, sezione 9, Scienze geologiche e paleontologiche. 1 [3], 59-62.
55. Pettijohn, F.J.; Potter, P.E.; Siever, R. (1987) Sand and sandstone. Springer-Verlag, New York. 617p.
56. Grossi, C.M.; Brimblecombe, P.; Esbert, R.M.; Alonso, F.J. (2007) Color changes in architectural limestones from pollution and cleaning. *Color Res. Appl.* 32 [4], 320–331. https://doi.org/10.1002/col.20322.

57. Cultrone, G.; Sánchez-Ibañéz, V. (2018) Consolidation with ethyl silicate: how the amount of product alters the physical properties of the bricks and affects their durability. *Mater Construcc*. 68 [332], e173. https://doi.org/10.3989/mc.2018.12817.
58. Zoghlami, K.; López-Arce; P., Zornoza-Indart, A. (2016) Differential stone decay at the Spanish tower façade of Bizerte, Tunisia. *J. Mater. Civ. Eng*. https://doi.org/10.1061/(ASCE)MT.1943-5533.0001774.
59. Zoghlami, K.; Gómez-Gras, D.; Álvarez, A.; Luxan, M.P. (2004) Intrinsic factors that condition the physical behavior and the durability of the Miocene sandstones used in the construction of the Roman aqueduct of Zaghouan-Carthage. *Mater. Construcc*. 54 [276], 37-49. https://doi.org/10.3989/mc.2004.v54.i276.254.
60. Dunčková, L.; Durmeková, T.; Adamcová, R.; Bednarik, M. (2022) Laboratory Assessment of Selected Protective Coatings Applied on Two Sandstone Types. *Coatings*. 12 [6], 761. https://doi.org/10.3390/coatings12060761.
61. González de Vallejo, L.; Ferrer, M.; Ortuño, L.; Oteo, C. (2012) (4th Ed). Ingeniería Geológica. Prentice Hall Pearson Educación, Madrid. 744p.
62. Saptono, S.; Kramadibrata, S.; Sulistianto, B. (2013) Using the Schmidt Hammer on rock mass characteristic in sedimentary rock at Tutupan coal mine. *Proc. Earth Planet. Sci*. 6, 390-395. https://doi.org/10.1016/j.proeps.2013.01.051.
63. Desarnaud, J.; Kiriyama, K.; Bicer Simsir, B.; Wilhelm, K.; Viles, H. (2019) A laboratory study of Equotip surface hardness measurements on a range of sandstones: What influences the values and what do they mean? *Earth Surf. Process. Landf.* 44 [7], 1419-1429. https://doi.org/10.1002/esp.4584.
64. Aoki, H.; Matsukura, Y. (2008) Estimating the unconfined compressive strength of intact rocks from Equotip hardness. *Bull. Engineer. Geol. Environ.* 67, 23-29. https://doi.org/10.1007/s10064-007-0116-z.